Electronic Supplementary Material (ESI) for Journal of Materials Chemistry A.

Supplementary Information

Constructing Z-Scheme WO_3/C_3N_4 heterojunctions with enlarged internal electric field and accelerated water oxidation kinetics for robust CO_2 photoreduction

Zhijia Song[a], Qian Chen[b], Zhiwei Sun[a], Kuan Chang[a], Zhaoxiong Xie[a,c], Qin Kuang[a,c,*]

[a]*State Key Laboratory of Physical Chemistry of Solid Surfaces, Collaborative Innovation Center of Chemistry for Energy Materials, Department of Chemistry, College of Chemistry and Chemical Engineering, Xiamen University, Xiamen 361005 (China)*

[b]*State Key Laboratory of Environment-Friendly Energy Materials, School of Materials and Chemistry, Southwest University of Science and Technology, Mianyang 621010, P. R. China.*

[c]*Innovation Laboratory for Sciences and Technologies of Energy Materials of Fujian Province (IKKEM), Xiamen 361005, China.*

E-mail: qkuang@xmu.edu.cn

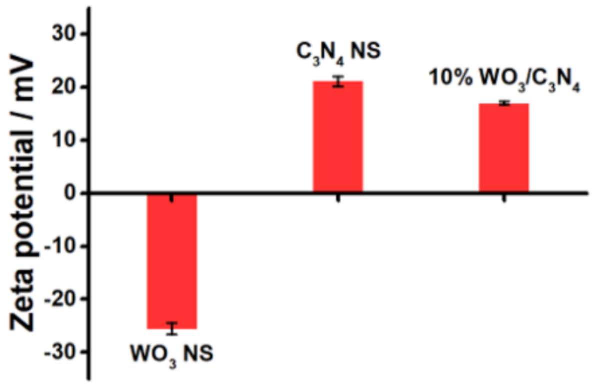

Figure S1. Zeta potential of WO_3 NS, C_3N_4 NS and 10%WO_3/C_3N_4 in deionized water.

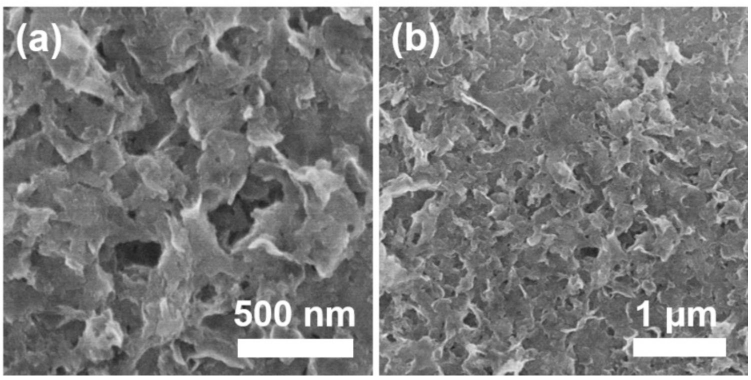

Figure S2. SEM images of C_3N_4 NS.

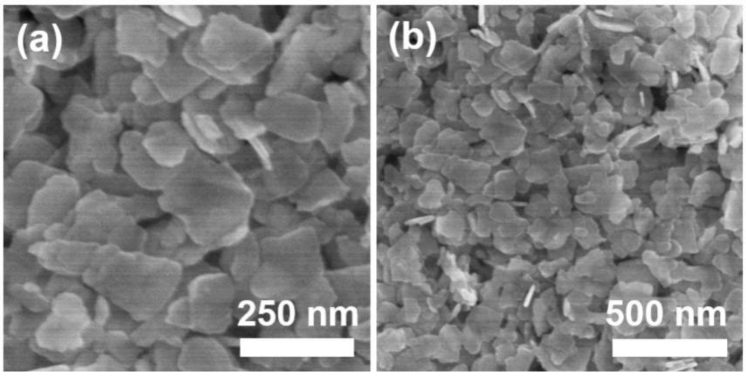

Figure S3. SEM images of WO_3 NS.

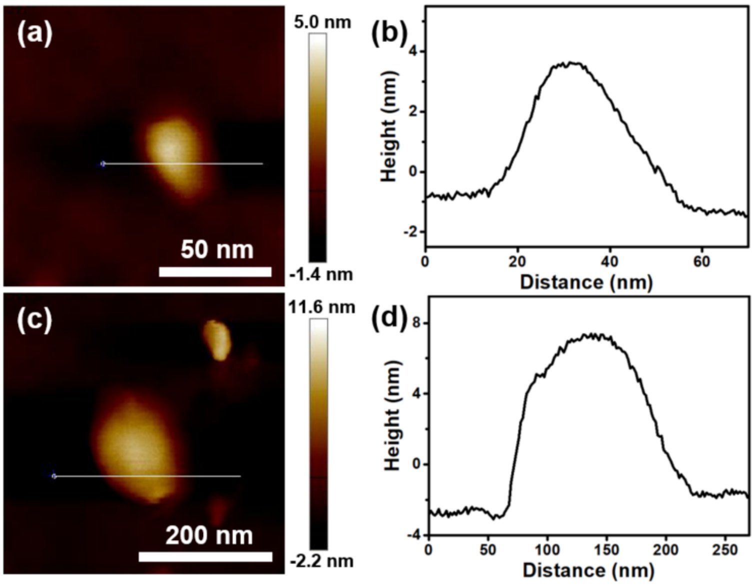

Figure S4. (a) AFM image and (b) the corresponding height profile of C_3N_4 NS; (c) AFM image and (d) the corresponding height profile of WO_3 NS.

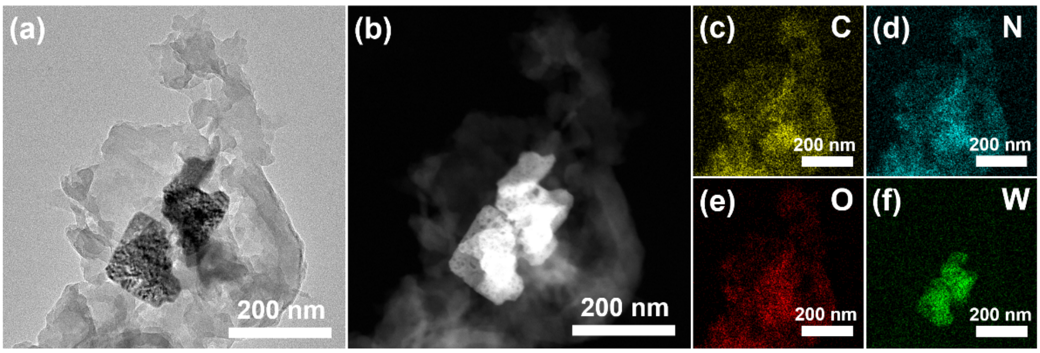

Fig. S5 (a) TEM image, (b) HAADF-STEM image and (c-f) EDS mapping images of 10%WO_3/C_3N_4.

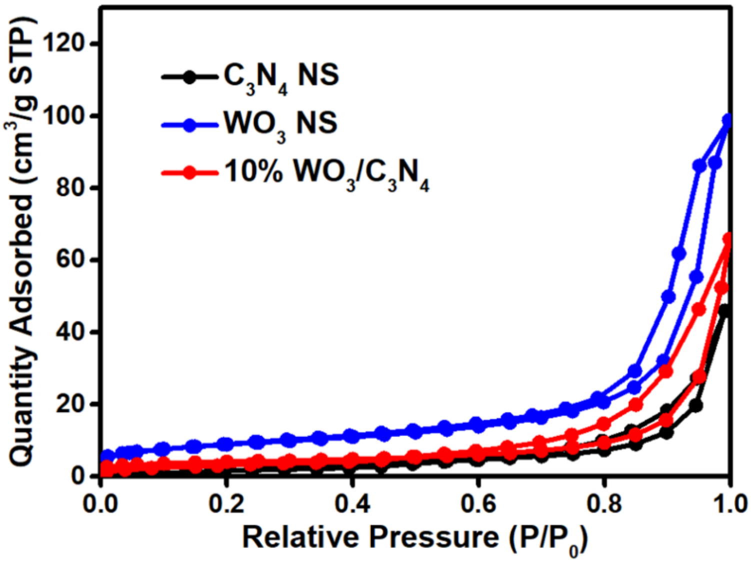

Figure S6. N_2 adsorption-desorption isotherms of C_3N_4 NS, WO_3 NS and 10%WO_3/C_3N_4.

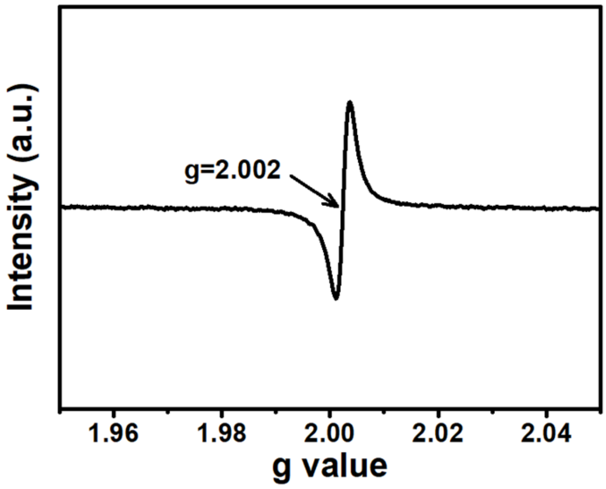

Figure S7. ESR spectra of WO_3 NS.

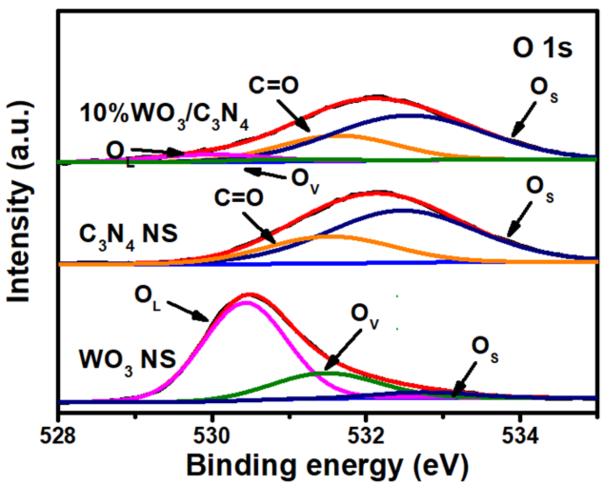

Figure S8. XPS spectra of O 1s in WO_3 NS, C_3N_4 NS, and 10%WO_3/C_3N_4.

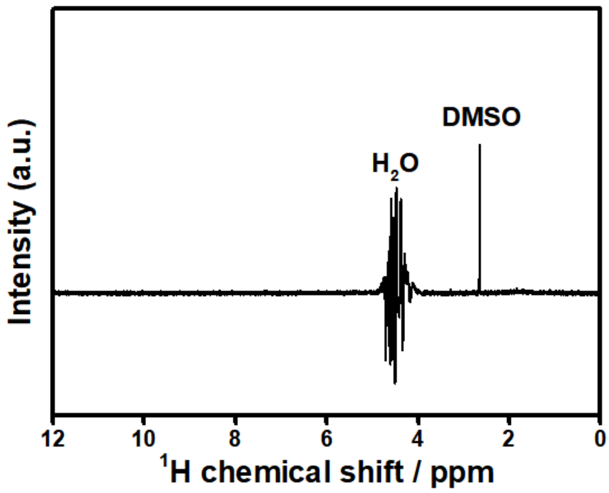

Figure S9. ^{1}H NMR spectra of the residual liquid obtained from CO_2 photoreduction for 10%WO_3/C_3N_4.

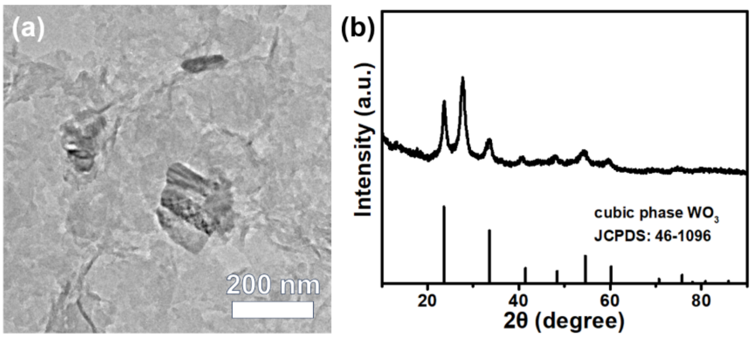

Figure S10. (a) TEM image and (b) XRD pattern of 10%WO_3/C_3N_4 after photocatalytic CO_2 reduction test.

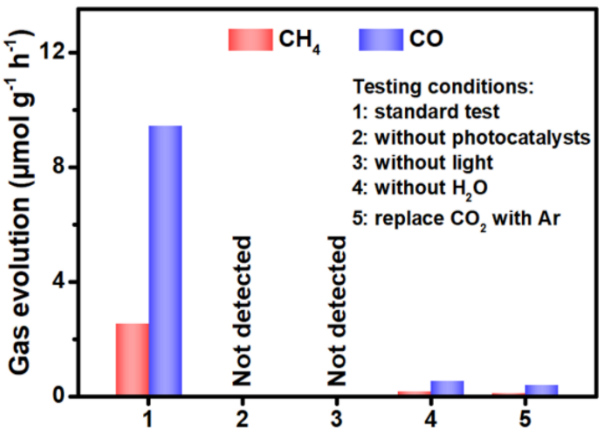

Figure S11. Control experiments and of 10% WO_3/C_3N_4 heterojunction.

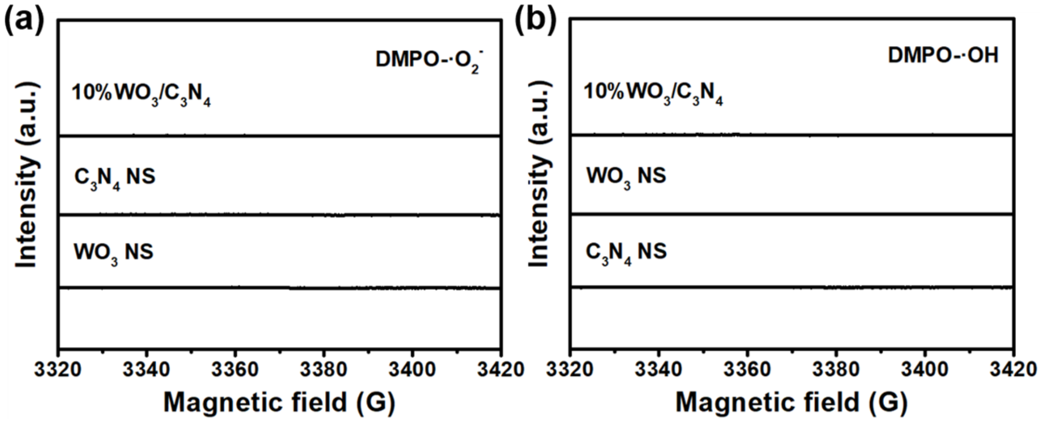

Figure S12. ESR spectra of (a) DMPO-▪O_2^- in methanol dispersion and (b) DMPO-▪OH in aqueous dispersion in the presence of C_3N_4 NS, WO_3 NS, and 10%WO_3/C_3N_4 in the dark.

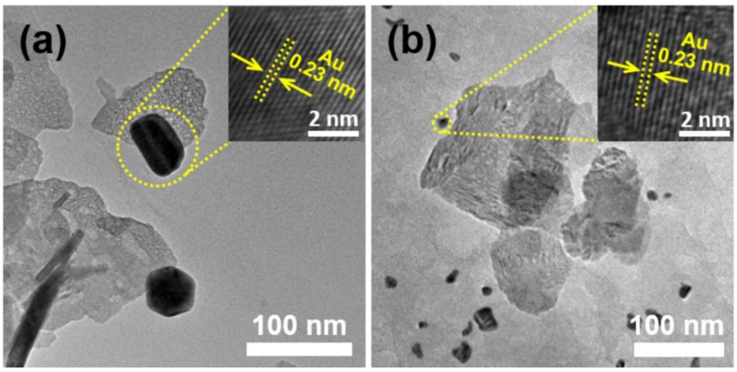

Figure S13.TEM images of (a) Au-WO_3-PD and (b) Au-10%WO_3/C_3N_4-PD.

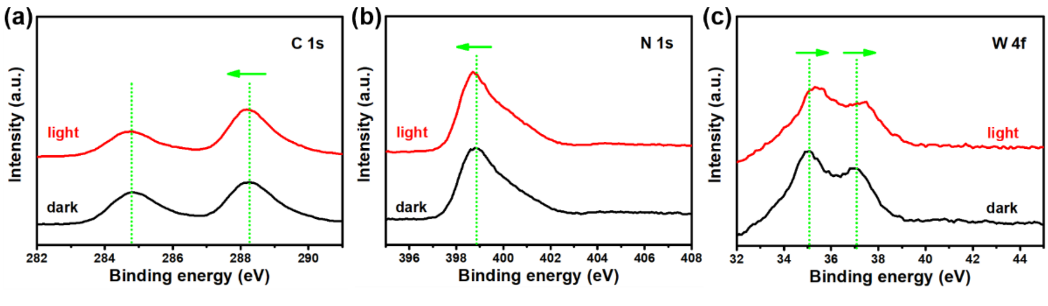

Figure S14. In situ irradiated XPS of (a) C 1s, (b) N 1s, and (c) W 4f for 10%WO_3/C_3N_4.

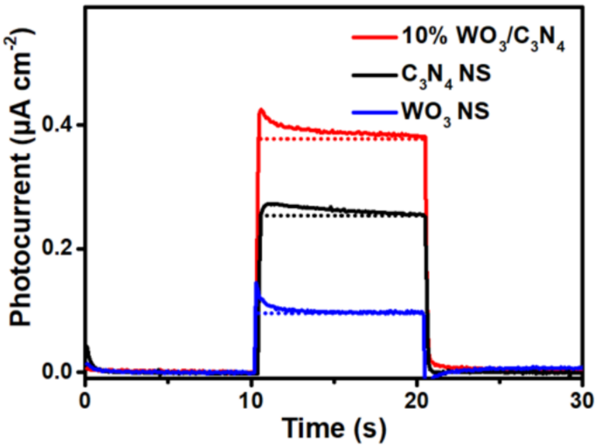

Figure S15. The transient photocurrent density of WO_3 NS, C_3N_4 NS and 10%WO_3/C_3N_4.

The internal electric field (IEF) magnitude was calculated by the equation developed by Kanata et al.: $F_S = \left(-2\rho V_S/\varepsilon\varepsilon_0\right)^{1/2}$, in which Fs is the IEF magnitude, ρ is the surface charge density, V_S is the surface voltage, ε is the low-frequency dielectric constant, and ε_0 is the permittivity of free space (ε and ε_0 are two constants). It can be found that the IEF magnitude is mainly determined by V_S and ρ. To assess their IEF magnitude, Vs was surveyed via open-circuit potential measurements, and ρ was determined through the transient photocurrent density measurements. Based on the previous report, integrating the measured transient photocurrent density minus the steady-state values of photocurrent with respect to time yields a value that is proportional to the number of negative charges accumulated at the surface. As depicted in Figure S17, the calculated integral areas for WO_3 NS, C_3N_4 NS, and 10%WO_3/C_3N_4were 0.039, 0.072, and 0.115, respectively. In other words, their surface charge densities were 0.039, 0.072, and 0.115 μC/cm^2, respectively. As depicted in Figure 4a, the OCP for WO_3 NS, C_3N_4 NS, and 10%WO_3/C_3N_4 were 37 mV, 52 mV, and 105 mV, respectively. Under the assumption that the intensity of WO_3 NS was normalized to “1”, the IEF magnitude were calculated to be 1.0, 1.6, and 2.9 for WO_3 NS, C_3N_4 NS, and 10%WO_3/C_3N_4, respectively, using the aforementioned equation.

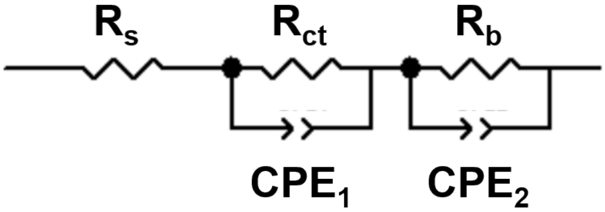

Figure S16. Equivalent circuit diagram for simulating the Nyquist plots of EIS.

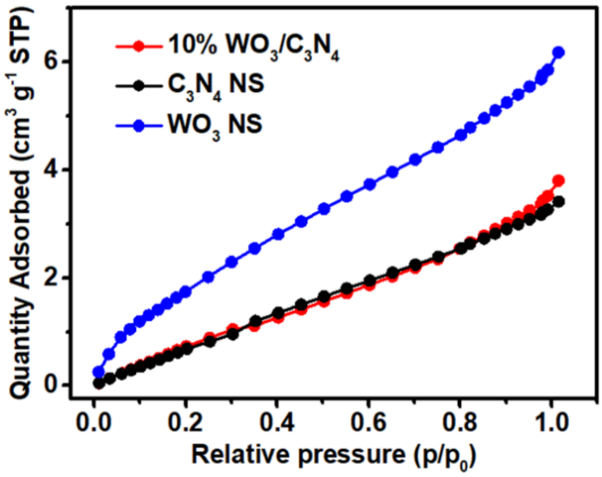

Figure S17. CO_2 physical adsorption capacity of C_3N_4 NS, WO_3 NS, and 10%WO_3 /C_3N_4.

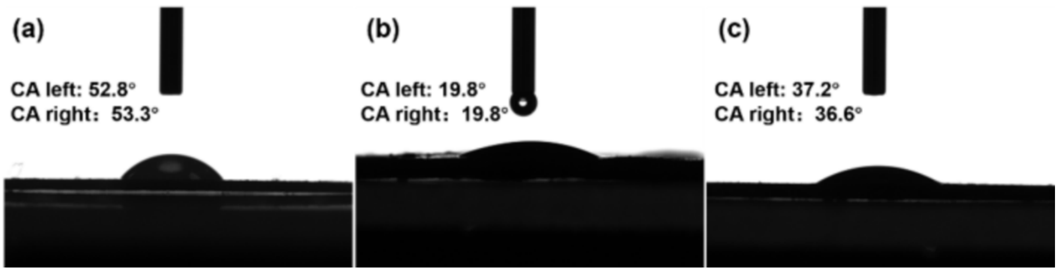

Figure S18. Water contact angle tests on the surface of (a) C_3N_4 NS, (b) WO_3 NS and (c) 10%WO_3 /C_3N_4.

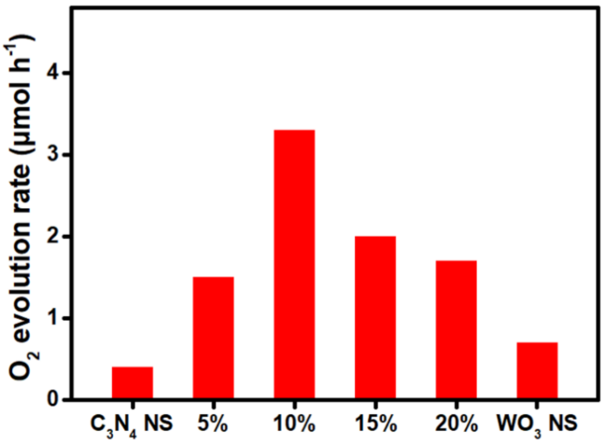

Figure S19. Conventional H_2O oxidation activities of as-prepared photocatalysts (The symbols 5%, 10%, 15% and 20% on the x-axis represent the 5%WO_3/C_3N_4, 10% WO_3/C_3N_4, 15% WO_3/C_3N_4 and 20% WO_3/C_3N_4 samples, respectively).

Table S1. A summary of recent C_3N_4-based materials for CO_2 photoreduction.

Materials	Experiment condition	Products ($\mu mol\ g^{-1}\ h^{-1}$)		Refenrence
		CH_4	CO	
10%WO_3/C_3N_4	300 W Xe lamp	2.6	9.4	This work
CeO_2/C_3N_4	300 W Xe lamp	0.60	8.99	*Sci. China Mater.*, 2023, **66**, 3165–3175
$BiVO_4/Ni_2P$/g-C_3N_4	300 W Xe lamp	0.11	6.40	*Appl. Catal. B: Environ.*, 2023, **337**, 122957
WO_x/Pt-g-C_3N_4	300 W Xe lamp	3.12	5.89	*Carbon*, 2023, **214**, 118337
$Ti_3C_2T_x$/CCN	300 W Xe lamp	1.4	0.73	*Chinese J. Catal.*, 2023, **53**, 109-122
$Bi_{19}S_{27}Br_3$/g-C_3N_4	300 W Xe lamp	0	12.87	*Appl. Catal. B: Environ.*, 2022, **307**, 121162
Cu modified g-C_3N_4	300 W Xe lamp	0.73	9.91	*J. Colloid Interface Sci.*, 2022, **622**,336-346
Pt@Def-CN	300 W Xe lamp	6.3	0.06	*Angew. Chem. Int. Ed.*, 2022, **134**, e202203063
Bi-BCN	300 W Xe lamp (380 nm cut-off filter)	0	8.17	*Chem. Eng. J.*, 2023, **478**, 147350
AUNB/g-C_3N_4	300 W Xe lamp (AM 1.5 filter)	0	5.5	*Chem. Eng. J.*, 2022, **430**, 132853
24-CN-EDA	300 W Xe lamp (420 nm<λ<780 nm)	0	1.72	*Chem. Eng. J.*, 2023, **455**, 140746

Table S2. The examine of photogenerated electron-hole balance in as-prepared samples.

Sample	Reduction products ($\mu mol\ g^{-1}\ h^{-1}$)		Oxidation products ($\mu mol\ g^{-1}\ h^{-1}$)	Electron-hole balance
	CH_4	CO	O_2	N_{e-}/N_{h+}
C_3N_4 NS	0.36	2.1	1.7	1.04
5%WO_3/C_3N_4	1.5	5.9	5.9	1.01
10%WO_3/C_3N_4	2.6	9.4	9.9	1.00
15%WO_3/C_3N_4	2.3	7.9	8.5	1.01
20%WO_3/C_3N_4	2.0	6.6	7.4	0.99
WO_3 NS	0	0	0	null